Proc. of the 30th International Slovak–Polish Scientific Conference on Machine Modelling and Simulations 2025

Experimental and Numerical Investigation of an Electromagnetic Impact Damper with Variable Mass

M. Żurawski*

Warsaw University of Technology, Faculty of Automotive and Construction Machinery Engineering, Narbutta 84, 02-524 Warsaw, Poland

Doi: 10.12693/APhysPolA.149.S16 *e-mail: mateusz.zurawski@pw.edu.pl

For many years, researchers have investigated the particle impact damper from the perspective of its design parameters and their influence on dynamic behavior and energy dissipation — key aspects studied in applied and theoretical physics. Numerous constructions have been proposed in the literature, including designs enabling adaptive tuning of the damper's internal volume. This study presents the design, experimental investigation, and physical modeling of an adaptive electromagnetic particle impact damper intended for vibration suppression. The experimental setup consists of a kinematic exciter, a cantilever beam equipped with the electromagnetic particle impact damper at its free end, and a comprehensive measurement system. The damper contains metallic granules that dissipate mechanical energy through inelastic collisions during beam oscillations, illustrating fundamental concepts such as energy transfer, dissipation mechanisms, and nonlinear dynamic interactions. A key innovation is the integrated electromagnet, which allows for selective blocking of the granules, enabling real-time control of the damper's effective mass. This adaptive control approach directly addresses the interplay between mass distribution and dynamic response, which is central to understanding physical systems. The experimental investigation explored how varying the proportion of freely moving granules influences the vibration characteristics of the system. Four test cases were defined, ranging from complete immobilization to partial release of the granular mass. The results demonstrated that increasing the number of free particles significantly enhances damping performance and reduces vibration amplitudes, confirming the critical role of granular dynamics in energy dissipation. To further analyze the system behavior, a reduced four-degree-of-freedom numerical model incorporating soft contact theory was developed. This model captures the nonlinear interactions between the moving particles and the beam structure, providing deeper insights into complex dynamic phenomena governed by fundamental physical principles. Comparisons with experimental data confirmed the model's accuracy and validated the effectiveness of the electromagnetic particle impact damper as a tunable and efficient damping solution. The findings confirm the electromagnetic particle impact damper concept as an effective and adaptable vibration mitigation approach. The ability to dynamically control the damper's effective mass represents a significant advancement over traditional particle impact dampers, introducing new opportunities for active control in engineering systems. This work not only demonstrates practical engineering benefits but also contributes to the broader understanding of adaptive dynamic systems and energy dissipation.

topics: damping of vibrations, mass redistribution, cantilever beam, particle impact damper

1. Introduction

Mitigation of the vibrations is essential to safeguard structural integrity and functional precision in aerospace, automotive, civil engineering, and high-tech equipment. Classic passive solutions, such as viscous dampers or tuned mass dampers (TMDs), are valued for robustness, but their fixed parameters make them susceptible to detuning when operating conditions drift [1–3]. As a consequence, research has shifted toward adaptive or semi-active concepts that can match the dynamic environment in real time without the energy demands of fully active systems.

Among passive devices, the particle impact damper (PID) has emerged as a low-cost, temperature-insensitive alternative. PID encloses metallic or ceramic granules inside a cavity attached to a vibrating host; energy is dissipated through inelastic inter-particle and particle–wall collisions that convert kinetic energy into heat and sound [4–6]. Compared to conventional viscoelastic treatments, PIDs exhibit high durability and maintain effectiveness over broad frequency and temperature ranges. Early empirical design studies established the effect of filling ratio, particle material, and mass ratio on damping performance, leading to the development of design curves and simplified predictive tools for

Fig. 1. Kinematic exciter.

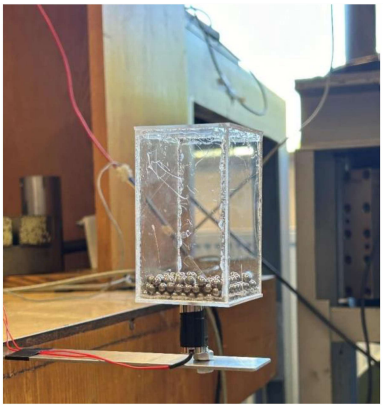

Fig. 2. Scheme of the test stand.

industry adoption [7–10]. More recent numerical work — including discrete-element and finite-element/discrete-element method hybrids hybrids — has clarified energy-dissipation pathways and enabled optimisation of enclosure geometries and particle mixtures [11–13].

Despite these advances, conventional PIDs remain intrinsically non-tunable once installed. To introduce adaptability, several modifications have been proposed:

- Variable-geometry or tuned PIDs (TPIDs) use moving walls or bellows to change cavity volume and therefore the clearance that governs particle flight time, achieving rapid frequency retuning in lightweight beams and plates [14, 15].
- Multi-compartment designs partition the cavity, broadening the effective bandwidth and improving robustness to detuning by redistributing the granular mass [16].
- Hybrid concepts combine particle damping with Coulomb friction or viscoelastic layers, leveraging complementary mechanisms to widen the effective operating range [17].
- Magneto-controlled or vacuum-packed granular dampers selectively lock or jam the particles using electromagnetic fields or under pressure, enabling semi-active adjustment of the effective moving mass or contact forces [18, 19].
- The latest adaptive tuned PID (ATPID) introduces feedback-controlled moving boundaries or electromagnetic particle arresters to provide fully programmable stiffness and damping in real time [20, 21].

Micro-gravity experiments and nonlinear time-frequency analyses further demonstrate that granular dampers retain efficiency even when collisional friction vanishes, underscoring their versatility for space applications [22–24]. Taken together, these developments position adaptive particle-based dampers as a promising bridge between simple passive and more complex active systems, offering tunable, fail-safe mitigation with minimal power demand and high reliability. The remaining work focuses on the electromagnetic particle impact damper (EMPID), a magnetically controlled variant of ATPID, and its ability to tailor damping performance online.

This paper is devoted to introducing a novel method for vibration attenuation in slender objects. The dynamics of the vibrating beam element are controlled in real time by a special system that enables the redistribution of the granular material introduced into the system. The proposed method of vibration damping can be placed among novel strategies of semi-active vibration attenuation. To reveal extraordinary features of the discussed concept, a typical cantilever beam subjected to kinematical excitation was used.

2. Test stand

The experimental setup (Fig. 1) consisted of a kinematic exciter, a cantilever beam, an EMPID damper, and a measurement system. The exciter was primarily composed of an electric motor that generated rotational motion. This motion was subsequently converted into vertical linear displacement by means of a disk with an eccentric mass. The excitation amplitude was determined by the eccentricity and was set to 10 mm. The cantilever beam was mounted to the exciter's holder, with the EMPID damper attached to its free end.

The measurement system included a data acquisition card and a laser displacement sensor, which enabled precise tracking of the displacement of the beam's free end. This configuration allowed for accurate observation and analysis of the system's dynamic behavior under periodic excitation.

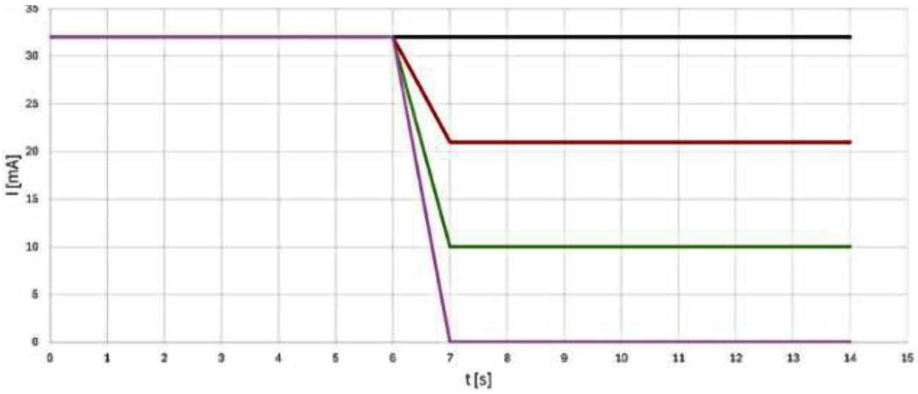

Fig. 3. Changes in the current.

The EMPID damper (Fig. 2) consists of a transparent casing and metallic granules enclosed within it. During vibrations, the granules move freely and undergo collisions both with each other and the inner walls of the damper. These interactions effectively contribute to the dissipation of mechanical energy, enhancing the damping characteristics of the system.

An integrated electromagnet was used to control the motion of the granules. By activating the electromagnet, it was possible to immobilize a portion of the granules within the enclosure. This feature enabled real-time control over the effective moving mass of the damper. Depending on the power supply and the strength of the generated electromagnetic field, a specific number of granules could be selectively locked, allowing for tunable damping properties during operation.

In the experimental study, four test cases were defined to investigate the influence of controlled granular motion on the system's dynamic response. Case 1 involved a fully activated electromagnet, which generated a magnetic field strong enough to completely immobilize all metallic granules inside the EMPID damper throughout the entire experiment. In contrast, Cases 2, 3, and 4 introduced a dynamic control scenario in which the electromagnetic field was altered at 5 s, allowing different proportions of the granules to move freely. The current supplied to the electromagnet was empirically adjusted to enable the motion of granules corresponding to 30% (Case 2), 60% (Case 3), and 100% (Case 4) of the total granular mass. This setup enabled real-time modulation of the damper's effective mass and energy dissipation capability. The corresponding current profiles used to trigger partial unlocking of the granules are presented in Fig. 3.

For all four cases, the dynamic response of the system was measured at the free end of the cantilever beam. The time histories of the beam's displacement for each case are presented in Fig. 4–7.

Case 1 (see Fig. 4) shows a clear and sustained resonant response. The amplitude gradually builds up, reaching a maximum displacement of $\approx \pm 0.22$ m around 6–8 s, after which it remains steady. The oscillations are symmetrical and exhibit minimal damping, indicating a continuous external excitation that matches the system's natural frequency. This Case represents a classical resonant condition with negligible energy loss. Case 2 (Fig. 5) also begins with an amplitude close to ± 0.22 m. However, after around 5 s, the amplitude gradually begins to decrease. This occurs because, within the enclosure, the granulate, representing 10% of the total system mass, remains in motion, introducing additional partial damping effects. Case 3 (Fig. 6) shows a more complex response, namely the system resonance amplitude rises for ≈ 5 s, after which the it decreases significantly and rapidly. The post-resonant oscillations persist, but at much lower amplitudes ($\sim \pm 0.05$ m), indicating higher damping ability. In this Case, the mass of the freely moving grains is equal 20% of the mass of the whole system. Case 4 (Fig. 7) shows the strongest damping effect among all cases. After reaching maximum amplitude, the amplitude rapidly decays into low-amplitude oscillations ($\sim \pm 0.03$ m). In this situation, all grains can move and collide. This allows us to introduce the most effective damping to the system for such a damper container.

3. Modeling

The mathematical model applied at this stage of the investigation was a simplified 4-degree-of-freedom (4-DOF) representation of the tested system. The cantilever beam was reduced to a single degree of freedom with equivalent mass `msm_sms`, stiffness `ksk_sks`, and damping coefficient `csc_scs`, and it was subjected to harmonic kinematic excitation `u(t)u(t)u(t)`. The metallic granular medium was modeled as three individual spheres moving vertically inside the damper enclosure. These spheres could collide only with the top and bottom walls of the damper, reflecting the dominant interaction mechanism observed in the physical setup.

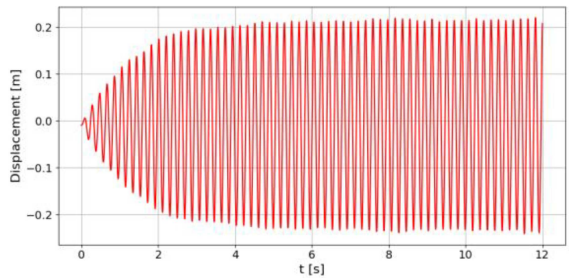

Fig. 4. Displacement of the free-end beam (Case 1).

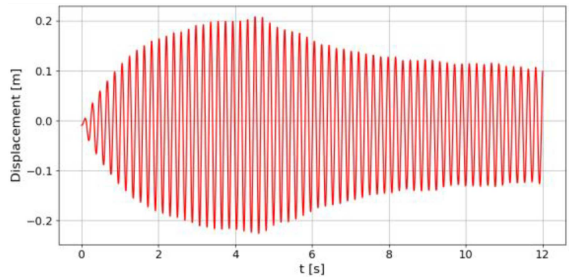

Fig. 5. Displacement of the free-end beam (Case 2).

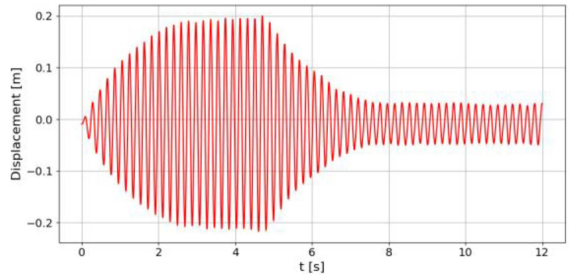

Fig. 6. Displacement of the free-end beam (Case 3).

A schematic representation of the model is shown in Fig. 8.

The equations of motion for this system are described by

$$m_s\ddot{x}_s + F_{ext} + Q_s + \sum_{i=1}^{j} \alpha_i \left(F_{c1,i} - F_{c2,i}\right) - \sum_{i=1}^{j} s_i F_{\mathrm{LOCK}} = 0, \tag{1}$$

$$m_{g,i}\ddot{x}_{g,i} - \alpha_i F_{c1,i} + \alpha_i F_{c2,i} + s_i F_{\mathrm{LOCK}} + Q_{g,i} = 0, \tag{2}$$

where m_s is the mass of the cantilever beam model and the term F_{ext} represents the external force arising from the harmonic kinematic excitation, modeled as $A\sin(\omega_0 t)$. The forces Q_s and $Q_{g,i}$ correspond to the gravitational forces acting on the beam and on each individual sphere, respectively. The terms $F_{c1,i}$ and $F_{c2,i}$ describe the contact forces between each sphere and the bottom and top walls of the damper housing.

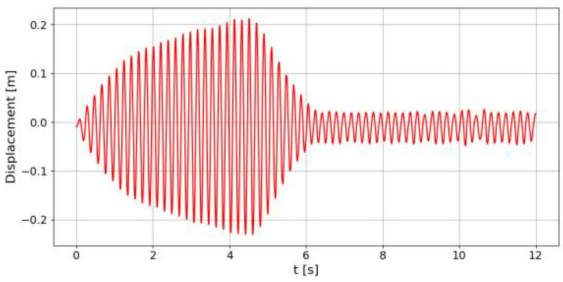

Fig. 7. Displacement of the free-end beam (Case 4).

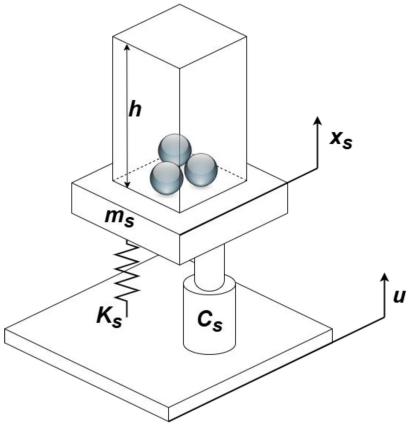

Fig. 8. Scheme of the theoretical model.

The term F_{LOCK} represents a substitute force that replaces the electromagnetic forces used in the experimental setup. This force is assumed to be sufficiently large to ensure that the acceleration of a given locked sphere matches the acceleration of the bottom wall of the damper, effectively constraining its motion. The parameters α_i and s_i are binary switching variables that determine whether a given sphere is free to move inside the damper or is locked and follows the motion of the structure ($\alpha_i = 0,\ s_i = 1$).

The contact forces between each sphere and the top or bottom wall are described using a nonlinear viscoelastic model, which takes the following form

$$F_{c1,i} = k_c\,\xi_{c1,i}^{3/2} + c_c\,\dot{\xi}_{c1,i}\,\xi_{c1,i}^{1/4}, \tag{3}$$

$$F_{c2,i} = k_c\,\xi_{c2,i}^{3/2} + c_c\,\dot{\xi}_{c2,i}\,\xi_{c2,i}^{1/4}, \tag{4}$$

$$\xi_{c1,i} = \max(0, d_i - x_{g,i} + x_s), \tag{5}$$

$$\xi_{c2,i} = \max(0, h - x_{g,i} + x_s), \tag{6}$$

where k_c and c_c denote the reduced contact stiffness and contact damping coefficient, respectively. These parameters are described in detail in paper [23]. The variables $\xi_{c1,i}$ and $\xi_{c2,i}$ represent the penetration (overlap) between a grain and either the lower or upper wall of the damper, depending on the direction of contact.

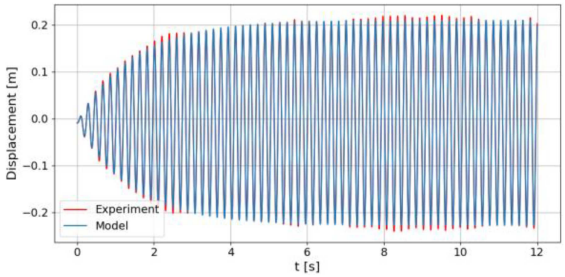

Fig. 9. Comparison of the experimental and theoretical displacement of the free-end beam (Case 1).

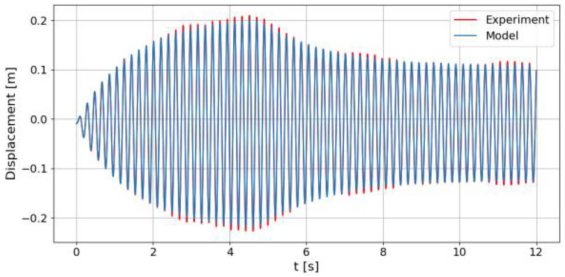

Fig. 10. Comparison of the experimental and theoretical displacement of the free-end beam (Case 2).

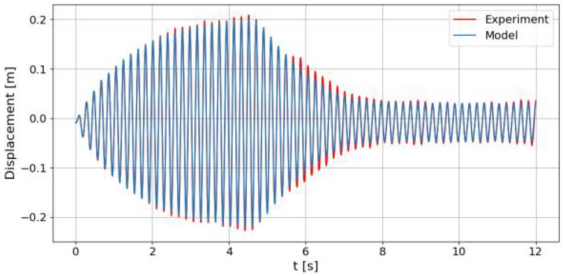

Fig. 11. Comparison of the experimental and theoretical displacement of the free-end beam (Case 3).

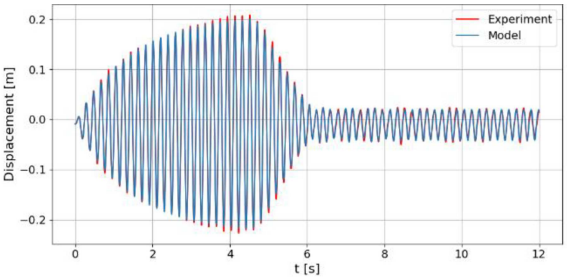

Fig. 12. Comparison of the experimental and theoretical displacement of the free-end beam (Case 4).

Parameters α_i and s_i take the forms as follows

$$\alpha_i = 1 - s_i = \begin{cases} 1 \ \rightarrow \text{grain can move,} \\ 0 \ \rightarrow \text{grain is blocked.} \end{cases} \tag{7}$$

When $\alpha_i = 1$ ($s_i = 0$), the individual sphere is not attached to the bottom wall of the damper and is free to move. When $\alpha_i = 0$ ($s_i = 1$), the selected sphere is locked and unable to move. In reference to the experimental study, at the fifth second of the simulation, the parameter s_i changes from 0 to 1. Depending on the specific case, this results in an increase in the freely moving granular mass from 0% to 10%, 20%, or 30% of the total system mass.

The set of four plots (Figs. 9–12) presents a comparative analysis of experimental and numerical displacement responses for different test cases. Each graph overlays the experimentally measured displacement (red) with the model-based numerical simulation (blue), enabling a direct visual assessment of the model's accuracy.

In Case 1 (see Fig. 9), the agreement between the experimental and numerical results is very good across the entire time range. The amplitude growth, steady-state oscillations, and phase alignment are all accurately captured. Very minor deviations occur during the initial transient phase, but they are practically negligible. Case 2 (Fig. 10) shows slightly more noticeable, but still very small, discrepancies in the decay phase. The model slightly underestimates the amplitude reduction after around 6 s, but the overall dynamics, including the shape and timing of the oscillations, remain appropriately reproduced. In Case 3 (Fig. 11), the experimental data features a pronounced decay starting around 5 s. The model successfully captures both the timing and the trend of this amplitude drop, although there is a small mismatch in the exact amplitude envelope during the decay. Nonetheless, phase and frequency alignment remain precise.

Case 4 (Fig. 12) exhibits the most abrupt decay after 5 s. The model replicates the response well, with only slight differences in amplitude damping visible in the post-resonance phase. Despite the stronger damping, the match remains close, particularly in frequency and oscillation timing.

Overall, in all four cases, the discrepancies between experimental and simulated responses are minimal. Differences, where they exist, are limited mostly to the amplitude envelope in the decay phase, and even there they remain small. The proposed model demonstrates acceptable agreement with experimental data. Its simplified formulation effectively captures the key dynamic behavior of the system, making it a useful and efficient tool for reproducing experimental responses with high accuracy.

4. Conclusions

This study introduced a novel prototype of an electromagnetic particle impact damper (EMPID), designed as an adaptive device for vibration reduction. The key innovation lies in the integration

of an electromagnet, which generates a controlled magnetic field inside the damper enclosure. This field enables selective immobilization of metallic granules, thus providing real-time control over the effective mass of the damper and its energy dissipation capability. Experimental results clearly demonstrate that the damping effectiveness is strongly dependent on the proportion of freely moving granular mass — higher mobility results in greater energy dissipation and faster decay of oscillations.

To complement the experimental investigation, a simplified four-degree-of-freedom (4-DOF) theoretical model was developed. In this model, the granular medium was abstracted as three individual spheres capable of vertical motion within the damper enclosure. These spheres could be selectively locked or released to emulate the effect of the electromagnetic field. The dynamic interaction between the grains and the damper walls was described using a nonlinear viscoelastic contact force model, capturing the essential features of impact-induced damping.

The numerical simulations closely matched the experimental measurements across all test cases, confirming the validity of the proposed theoretical framework. The ability of the model to accurately reproduce the amplitude decay, phase response, and transient behavior of the system highlights its potential as a predictive tool for design and optimization.

Overall, the EMPID represents a significant advancement over traditional particle impact dampers (PIDs) by enabling adaptive and programmable control of damping performance. Its modular design, combined with the ability to regulate the internal dynamics through magnetic actuation, opens new possibilities for application in systems operating under variable loading or frequency conditions.

Future research directions include the development of hybrid EMPID systems that combine control over the granular mass with variable-volume enclosures, allowing for simultaneous tuning of particle mobility and impact dynamics. Such enhancements would enable even broader control authority and greater versatility in complex structural applications.

References

[1] T.T. Soong, G.F. Dargush, *Passive Energy Dissipation Systems in Structural Engineering*, Wiley, 1997.

[2] J.P. Den Hartog, *Mechanical Vibrations*, 4 ed., McGraw-Hill, 1956.

[3] A. Preumont, *Vibration Control of Active Structures: An Introduction*, Springer, 2011.

[4] H.V. Panossian, *J. Vib. Acoust.* **114**, 101 (1992).

[5] R.D. Friend, V.K. Kinra, *J. Sound Vib.* **233**, 93 (2000).

[6] K.S. Marhadi, V.K. Kinra, *J. Sound Vib.* **283**, 433 (2005).

[7] Z.W. Xu, K.W. Chan, W.H. Liao, *Shock Vib.* **11**, 647 (2004).

[8] M.Y. Yang, G.A. Lesieutre, S.A. Hambric, G.H. Koopmann, *Noise Control Eng. J.* **53**, 5 (2005).

[9] M. Saeki, *J. Sound Vib.* **251**, 153 (2002).

[10] K. Zhang, T. Chen, X. Wang, J. Fang, *J. Sound Vib.* **364**, 30 (2016).

[11] N. Meyer, R. Seifried, *Comput. Part. Mech.* **8**, 681 (2021).

[12] L. Gagnon, M. Morandini, G.L. Ghiringhelli, *J. Sound Vib.* **459**, 114865 (2019).

[13] Z. Lu, Z. Wang, S.F. Masri, X. Lu, *Struct. Control Health Monit.* **25**, e2058 (2018).

[14] H. Ye, Y. Wang, B. Liu, X. Jiang, *Appl. Sci.* **9**, 2912 (2019).

[15] M. Żurawski, R. Zalewski, *Appl. Sci.* **10**, 6334 (2020).

[16] A. Papalou, *Vibration* **6**, 556 (2023).

[17] M.A. Akbar, W.-O. Wong, E. Rustighi, *Machines* **11**, 545 (2023).

[18] M. Żurawski, R. Zalewski, *Materials* **15**, 6170 (2022).

[19] R. Faraj, G. Mikułowski, R. Wiszowaty, *Smart Mater. Struct.* **29**, 115008 (2020).

[20] M. Żurawski, C. Graczykowski, R. Zalewski, *J. Sound Vib.* **564**, 117799 (2023).

[21] X. Guo, Y. Zhu, Z. Luo, D. Cao, J. Yang, *Appl. Math. Mech.* **44**, 2163 (2023).

[22] M.N. Bannerman, J.E. Kollmer, A. Sack, M. Heckel, P. Mueller, T. Pöschel, *Phys. Rev. E* **84**, 011301 (2011).

[23] M. Sánchez, C.M. Carlevaro, *J. Sound Vib.* **332**, 2070 (2013).

[24] C. Xu, N. Zheng, L.-S. Li, Q.-F. Shi, *Powder Technol.* **297**, 367 (2016).